Small-Molecule Targeting of Heat Shock Protein 90 Chaperone Function: Rational Identification of a New Anticancer Lead

Massimiliano Meli,[†,‡] Marzia Pennati,[‡] Maria Curto,[‡] Maria Grazia Daidone,[‡] Janet Plescia,[§] Sam Toba,[||] Dario C. Altieri,[§] Nadia Zaffaroni,[‡] and Giorgio Colombo*,[†]

Istituto di Chimica del Riconoscimento Molecolare, Consiglio Nazionale delle Ricerche, Via Mario Bianco 9, 20131 Milano, Italy, Istituto Nazionale Studio e Cura Tumori, Department of Experimental Oncology, Unit 10, Via Venezian 1, 20133 Milano, Italy, Department of Cancer Biology and the Cancer Center, University of Massachusetts Medical School, Worcester, Massachusetts 01605, and Accelrys, Rational Drug Discovery, San Diego, California 92121

Received July 17, 2006

Heat shock protein 90 (Hsp90) is a significant target in the development of rational cancer therapy due to its role at the crossroads of multiple signaling pathways associated with cell proliferation and cell viability. Here we present a combined structure- and dynamics-based computational design strategy, taking the flexibility of the receptor and of a lead peptidic antagonist into account explicitly, to identify the nonpeptidic small molecule 5-aminoimidazole-4-carboxamide-1-β-D-ribofuranoside (AICAR) as a structurally novel inhibitor of Hsp90. The compound is selected to bind the Hsp90 N-terminal domain, mimicking the chemical and conformational properties of the recently described peptidic antagonist of the survivin–Hsp90 complex, shepherdin [Plescia et al. *Cancer Cell* **2005**, *7*, 457–468]. Experimental tests show that AICAR binds the Hsp90 N-domain, destabilizes multiple Hsp90 client proteins in vivo, including survivin, and exhibits antiproliferative and proapoptotic activity in multiple tumor cell lines, while not affecting proliferation of normal human fibroblasts. We propose that AICAR represents a viable lead for further development of anticancer drugs with wide therapeutic opportunities.

Introduction

Cancer therapy now aims at disabling oncogenic pathways that are selectively operative in tumor cells, so as to spare normal tissues and limit side effects in humans. This "targeted therapy" relies on a better understanding of cancer genes, particularly those implicated in tumor cell proliferation and survival.[1] Accordingly, targeted inhibition of the Bcr-Abl kinase with small molecule antagonists has produced dramatic clinical responses in malignancies driven by this oncogene.[2–4] However, such approaches may not be immediately available for the majority of tumors where multiple molecular abnormalities and genetic instabilities may elude the identification of one single, disease-driving oncogene.[1] Conversely, pathways that intersect multiple essential functions of tumor cells may provide wider therapeutic opportunities. A prime target for this strategy is the heat shock protein 90 (Hsp90), a molecular chaperone that oversees the correct conformational development of polypeptides and protein refolding through sequential ATPase cycles and stepwise recruitment of cochaperones. This adaptive pathway contributes to the cellular stress response to environmental threats, including heat, heavy metal poisoning, hypoxia, and so on, and is extensively exploited in cancer, where Hsp90 ATPase activity is upregulated ∼100-fold.[5] The repertoire of Hsp90 client proteins is restricted mainly to growth-regulatory and signaling molecules, especially kinases and transcription factors, which may contribute to tumor cell maintenance.[5,6] Therefore, targeted suppression of Hsp90 ATPase activity with a small molecule inhibitor, the benzoquinone ansamycin antibiotic 17-allylamino-17-demethoxygeldanamycin (17-AAG), has shown promising anticancer activity in preclinical models and has recently completed safety evaluation in humans.[7,8] One Hsp90 client protein with critical roles in tumor cell proliferation and cell viability is survivin, an inhibitor of apoptosis (IAP) protein selectively overexpressed in cancer.[9,10] Accordingly, targeting the survivin–Hsp90 complex may provide a strategy to simultaneously disable multiple signaling pathways in tumors, and a peptidomimetic antagonist of this interaction structurally different from 17-AAG, shepherdin, inhibited the chaperone activity and exhibited potent and selective anticancer activity in preclinical models.[11]

In this study, we have used shepherdin (LFACGSSHK, all D-amino acids) as a scaffold to rationally identify low-molecular-weight compounds that may act as structurally novel Hsp90 antagonists (Figure 1). We built a three-dimensional pharmacophore to screen a database of nonpeptidic structures, and we identified a novel antagonist of Hsp90 chaperone function with promising anticancer activity. The results presented here open the possibility to expand the molecular diversity space of Hsp90 antagonists.

Materials and Methods

Simulation Setup, Docking Experiments, and Molecular Dynamics (MD) Refinement of Hsp90/Shepherdin Complex. MD simulations of shepherdin in isolation in solution were described in ref 11. The docking procedure can be summarized as follows: the representative of the main conformational clustering for shepherdin structures (β-hairpin) was subjected to blind docking experiments on the putative N-terminal Hsp90 receptor using the program AutoDock.[12] The crystal structure of the protein was taken from the protein data bank (pdb code 1YET).[13] The original X-ray structure contains the ligand GA, which was removed from the active site to yield the apo-open form of Hsp90.

Mass-centered grid maps were generated with 0.25 Å spacing by the program Autogrid for the whole Hsp90 protein target. Lennard–Jones parameters 12–10 and 12–6 (the default param-

* To whom correspondence should be addressed. Tel.: +39-02-28500031. Fax: +39-02-28901239. E-Mail: g.colombo@icrm.cnr.it.
† Istituto di Chimica del Riconoscimento Molecolare.
‡ Istituto Nazionale Studio and Cura Tumori.
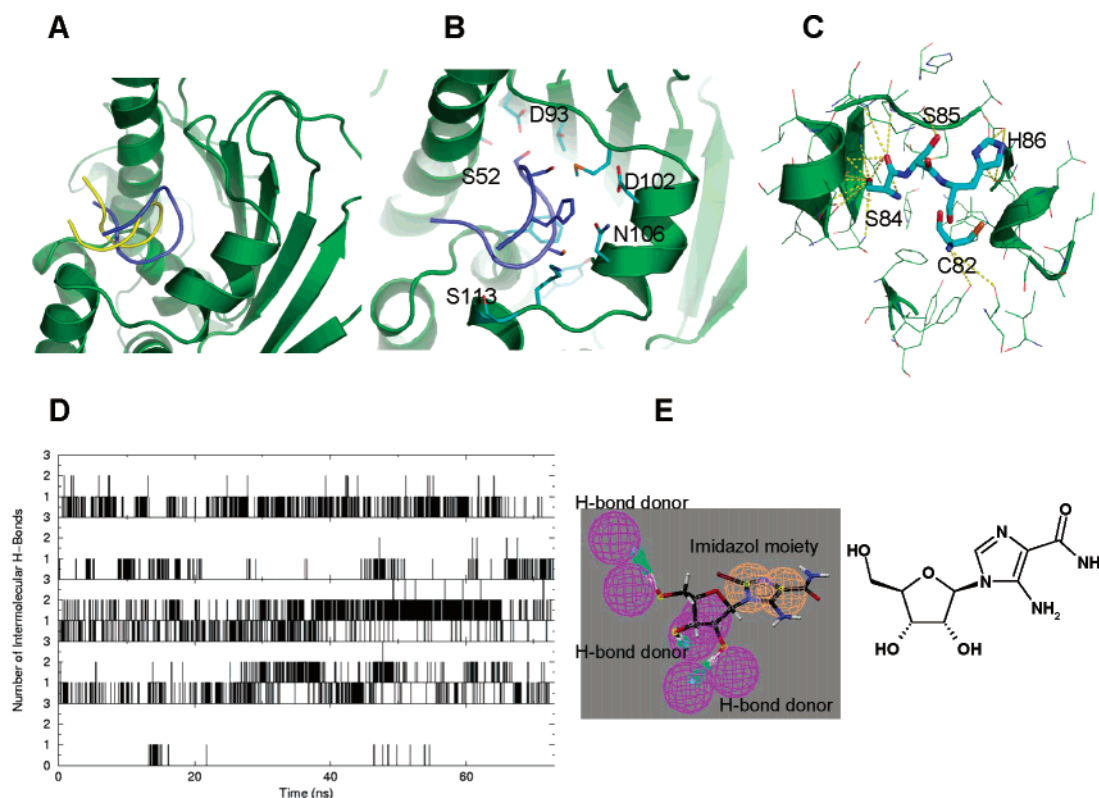§ University of Massachusetts Medical School.
|| Accelrys.

Figure 1. Identification of shepherdin/Hsp90 binding determinants. Determination of pharmacophore model and AICAR identification. (A) Structure of the MD-refined docked complex between shepherdin and the N-domain of Hsp90 (green). Initial (yellow) and final (blue) structure of shepherdin within the ATP-binding pocket of Hsp90 with two different orientations. (B) Side-chain groups of Hsp90 responsible for the main interactions with shepherdin. (C) Close-up of the groups of shepherdin (colored by atom) responsible for stabilizing interactions with Hsp90 (green). (D) Time evolution of the H-bonding interactions between Hsp90 and shepherdin groups (from top to bottom) γ-OH of S84, γ-OH of S85, Nϵ of H86, Nδ−H of H86, and SH of C82. (E) The pharmacophoric hypothesis mapped on the 3D structure of AICAR and its molecular structure (5-aminoimidazole-4-carboxamide-1-β-D-ribofuranoside, AICAR).

eters in the program package) were used for modeling H-bonding and Van der Waals interactions, respectively. The distance-dependent dielectric permittivity of Mehler and Solmajer[14] was used for calculation of the electrostatic grid maps. The Lamarckian genetic algorithm (LGA) and the pseudo-Solis and West methods were applied for minimization using default parameters. The number of generations was set to 25 million in all runs, and the stopping criterion was, therefore, defined by the total number of energy evaluations. Random starting positions on the entire protein surface, random orientations, and torsions (flexible ligand only) were used for the ligand. A total of 350 runs were performed. At the end of the docking runs, the conformations of the ligand peptide were listed in increasing energy order. Subsequently, the ligand conformation with the lowest energy was used as the reference, and all conformations with a center of mass to center of mass distance of <2.5 Å from the reference were assigned to the first cluster. Once a conformation was assigned to a cluster, it was not used again for other energetically less-favorable clusters. Then the process was repeated for all hitherto unclassified conformations until all conformations were put in a cluster, thus identifying 49 structural clusters corresponding to different free-energy values for the complex. Root-mean-square deviation (rmsd) values among different docked conformations are reported in the Supporting Information, Figures S1 and S2. Most of the docked structures shared common conformational characteristics, which are prototypically represented by the structure of the global minimum of the complex. This structure was chosen for further studies via all-atom, explicit solvent MD simulations.

The shepherdin/Hsp90 complex was first solvated with water in a periodic truncated octahedron, large enough to contain the peptide and 0.9 nm of solvent on all sides. The protonation and charge states of the side chains of the ligand and the receptor were chosen to be consistent with the solution conditions of the experiments:

NH groups were considered as having a +1 charge and carboxylic groups were considered as having a −1 charge. The system was found to have a total charge of −8. All solvent molecules within 0.15 nm of any peptide atom were removed. Eight Na$^+$ counterions were added to the system. Two different sets of initial velocities obtained from a Maxwellian velocity distribution at the desired temperature of 300 K were used to yield two different production runs of 54 and 73 ns, respectively.

In each case, the system was initially energy minimized with a steepest descent method for 1000 steps. In all simulations, the temperature was maintained close to the intended value of 300 K by weak coupling to an external temperature bath,[15] with a coupling constant of 0.1 ps. The Hsp90/shepherdin complex and the rest of the system were coupled separately to the temperature bath. The GROMOS96 force field[16,17] and the simple point charge (SPC)[18] water model were used. The LINCS algorithm[19] was applied to constrain all bond lengths. For the water molecules, the SETTLE algorithm[20] was used. A dielectric permittivity, $\epsilon = 1$, and a time step of 2 fs were used. A cutoff was taken for the calculation of the nonbonded Van der Waals interactions. The cutoff radius was set at 0.9 nm. The calculation of electrostatic forces utilized the PME implementation of the Ewald summation method.[21] In each simulation, the density of the system was adjusted by performing the first equilibration runs in NPT condition by weak coupling to a bath of constant pressure ($P_0 = 1$ bar, coupling time $\tau_{\_P} = 0.5$ ps).[15] All simulations were equilibrated by 50 ps of MD runs with position restraints on the protein and ligand to allow relaxation of the solvent molecules. These first equilibration runs were followed by another 50 ps run without position restraints on the solute. The production runs using NVT conditions, after equilibration, were 54 and 73 ns long. All the MD runs and the analysis of the trajectories were performed using the GROMACS software pack-

Table 1. Orientations of Pharmacophoric Groups[a]

functional groups	minimum dihedral value (degrees)	maximum dihedral value (degrees)
Ser84_γOH -- Ser85_γOH	260.7	290.7
Ser84_γOH -- Cys82_SH	247.0	277.0
Ser85_γOH -- Cys82_SH	184.0	214.0
Cys82_SH -- Imidaz_His86	27.2	57.2
Ser84_γOH -- Imidaz_His86	133.7	163.7
Ser85_γOH -- Imidaz_His86	43.9	73.9

[a] Minimum and maximum values of dihedral angles between functional groups used for PHARM1. The definitions of dihedral are reported in Materials and Methods.

Table 2. Distances between Pharmacophoric Groups[a]

functional groups	avg. dist. (nm)
Ser84_γOH -- Ser85_γOH	0.71 ± 0.09
Ser84_γOH -- Cys82_SH	0.90 ± 0.12
Ser85_γOH -- Cys82_SH	0.63 ± 0.15
Cys82_SH -- Imidaz_His86	0.77 ± 0.21
Ser84_γOH -- Imidaz_His86	1.11 ± 0.09
Ser85_γOH -- Imidaz_His86	0.52 ± 0.14

[a] Average distances and standard deviation from MD simulations used to define distances between functional groups in PHARM1.

age.[22] Configurations of the receptor−ligand complex were saved every 4 ps for subsequent statistical analysis.

Conformational cluster analysis of the two trajectories was performed using the method described by Daura et al.:[23] count the number of neighbors using a cutoff of 0.20 nm rmsd between the optimal backbone superposition of different structures, and take the structure with the largest number of neighbors with all its neighbors as cluster and eliminate it from the pool of clusters. This procedure is repeated for the remaining structures in the pool. The most populated cluster, representative of the most visited structures in the MD simulations, for the Hsp90/shepherdin complex is represented in Figure 1 and was used as a template for pharmacophore design. The relative distances and orientations (dihedral angles) among the different groups were evaluated as averages over the whole trajectories. For dihedral calculations, the angles were defined as the solid angles in 3D space determined by the vectors that unite the O−H or S−H atoms in Ser or Cys or by the vector normal to the imidazole plane of histidine.

Pharmacophore Generation. Three different pharmacophore models were built and labeled PHARM1, PHARM2, and PHARM3 based on the results of MD simulations. The conformation of shepherdin and the orientations of its side-chain functional groups in the most populated structural cluster from MD trajectories of the complex were used as structural template (Figure 1C,E). The distributions of dihedral values (Table 1) and distances (Table 2) among critical functionalities were used to define upper and lower boundaries for geometric constraints. The HypoGen Module of the Catalyst program from Accelrys[24] was used for this purpose. For PHARM1, a four-point model was created by assembling three H-bond donors mapped over the two Ser γ -OH and the Cys SH groups, and one imidazole moiety mapped over the imidazole ring of His of shepherdin. The torsional and distance restraints reported in Tables 1 and 2 were added to restrict the database search. Furthermore, we imposed location constraints (the volume in which the functions can reside), specifying the radius of the spheres according to Catalyst's defaults. PHARM2 and 3 were constructed in a similar way, augmenting PHARM1 with an aromatic function centered on the position of the Phe80 benzene ring and a hydrophobic function centered on the S atom of Cys82 (PHARM2) or by the presence of a positive charge mapped on the position of the ammonium group of Lys87 (PHARM3). These were used as queries for a search in the NCI_3D database using the database search module of Catalyst.

Small Molecule/Hsp90 Docking and MD Refinement of the Complex. The small molecule lead, 5-aminoimidazole-4-carbox-

amide-1-β-d-ribofuranoside[25] (AICAR, Figure 1E), identified as active through the procedure described above and experimental tests in different tumor and normal cell lines, was docked on Hsp90, using the Autodock program and the same protocol as described for shepherdin. The clustering procedure identified one dominant set of conformations for the AICAR/Hsp90 complex, including the free-energy minimum structure. The latter structure was used as the starting structure for subsequent MD refinement of the complex in explicit water. MD was carried out once again following the procedure described above for the shepherdin/Hsp90 complex for a total of 100 ns. The resulting trajectory was analyzed in terms of the main interactions (hydrogen bonding, favorable contacts, etc.) taking place during the simulation time. This information can be used to define possible structure−activity relationships for the AICAR/Hsp90 complex with the aim to design derivatives with improved activities and pharmacological properties.

Recombinant Proteins and Binding Studies. The N-domain (residues 1−272) or C-domain (residues 629−732) of Hsp90 were expressed as recombinant fusion proteins and purified after removal of the GST frame by thrombin cleavage, as described previously. Binding of AICAR to recombinant Hsp90 fragments was carried out by ELISA. Briefly, increasing concentrations of AICAR (Sigma-Aldrich, St. Louis, MO; 0.02−5 mM) were immobilized on plastic microtiter wells, blocked in 3% gelatin, and further mixed with recombinant N- or C-domain of Hsp90 (1 μg/mL) for 2 h at 310 K (37 °C). After washes, binding of the various Hsp90 fragments to AICAR-coated wells was detected using domain-specific antibodies to Hsp90 and quantified by absorbance at 405 nm. In another series of experiments, AICAR (5 mg/mL) was coupled to Sepharose beads (1 mL) and used to fractionate HeLa cell extracts prepared in 20 mM Tris, pH 7.2, 0.5% deoxycholate, 1% Triton X-100, 0.1% SDS, 150 mM NaCl, 1 mM EDTA plus protease inhibitors. After washes, bound proteins were eluted in 0.1 M glycine, pH 2.5, immediately buffered to neutrality, separated on SDS polyacrylamide gels, and analyzed by Western blotting. Fractionation of HeLa cell extracts over uncoupled Sepharose beads was used as control.

Cell Lines and Cultures. Androgen-independent adenocarcinoma (DU145), cervical carcinoma (HeLa), and melanoma (JR8) cell lines were grown in RPMI-1640 medium (BioWhittaker, Verviers, Belgium) supplemented with 10% fetal bovine serum. The normal human lung fibroblast cell line (WI38) was grown in DMEM medium (BioWhittaker) supplemented with 5% fetal bovine serum. All cell lines were maintained as monolayers at 310 K (37 °C) in a 5% CO_2 humidified atmosphere in air.

Growth Inhibition and Apoptosis Assays. After harvesting in the logarithmic growth phase, cells were seeded in 6-well plates for 24 h and then exposed to various concentrations of AICAR or 17-AAG for 72 h at 310 K (37 °C) in a 5% CO_2 humidified atmosphere. At the end of treatment, cells were washed twice with PBS, trypsinized, and counted in a particle counter (Coulter Counter, Coulter Electronics, Luton, U.K.). Each experimental point was run in triplicate. The results were expressed as the number of cells in treated samples compared with control samples.

For determination of apoptosis, cells were fixed in 70% (v/v) ethanol, stained with a solution containing 50 μg/mL propidium iodide, 10 mg/mL RNase, and 0.1% (v/v) Tween20 for 30 min at room temperature, and analyzed with a FACScan flow cytometer (Becton Dickinson, Sunnyvale, CA). A flow-cytometric sub-$G_{0/1}$ peak was detected on DNA plots using the CellQuest software according to the Modfit model (Becton Dickinson). In parallel, an aliquot of the propidium iodide-stained cell suspension was spotted onto slides and assessed for typical apoptotic nuclear morphology (nuclear shrinkage, condensation and fragmentation) under a fluorescence microscope with appropriate filter combinations. Apoptotic cells were determined by two independent observers scoring at least 500 cells in each sample.

Caspase-3 and caspase-9 activities were measured as the ability to cleave the specific substrates *N*-acetyl-Leu-Glu-His-Asp-pNA (LEHD-pNA) and *N*-acetyl-Asp-Glu-Val-Asp-pNA (DEVD-pNA) by means of the APOPCYTO/caspase-9 and APOPCYTO/caspase-3

assay kits (Medical and Biological Laboratories, Naka-ku Nagoya, Japan) according to the manufacturer's instructions.

Analysis of Hsp90 Chaperone Function. To monitor changes in Hsp90 client proteins, cells were harvested and solubilized in lysis buffer (0.01% NP40, 10 mM Tris [pH 7.5], 50 mM KCl, 5 mM MgCl$_2$, 2 mM DTT, 20% glycerol plus protease inhibitors) plus four pulses on a sonicator (10 s each) at 50 J/Watt-sec, alternated by 30-sec intervals on ice, and analyzed by Western blotting primary antibodies specific for survivin (Novus Biologicals, Littleton, U.K.), Hsp90, Hsp70, CDK-6, Raf-1, Neu (Santa Cruz Biotechnology, Santa Cruz, CA), and Akt (Cell Signaling Technology, Danvers, MA). Alternatively, lysates were immunoprecipitated with a rabbit polyclonal Hsp90 antibody (Santa Cruz Biotechnology) precoupled to 8 μL of a 50% slurry of protein-G-agarose beads for 1 h at 4 °C. After washes, the immunoprecipitates were analyzed for telomerase activity by telomeric repeat amplification protocol (TRAP) assay using the TRAPeze kit (Intergen Co., Oxford, U.K.). Each reaction product was amplified in the presence of a 36-bp internal TRAP assay standard (ITAS). Quantitative analysis was performed with the Image-QuanT software (Molecular Dynamics) as previously described.[26]

Statistical Analysis. Data were analyzed using the two-sided unpaired Student's *t* test. A *p* value of 0.05 was considered as statistically significant.

Results

Characterization of Hsp90/Shepherdin Binding Interface. The dominant conformations of shepherdin in solution were investigated through all-atom, explicit solvent MD simulations for a total time span of 400 ns. Statistical cluster analysis showed that shepherdin displays one main conformation, characterized by the presence of a turn involving residues G83-S84 and an overall hairpin geometry (see ref 11 for details). The remaining clusters were mainly extended conformations, with the peptide backbone groups involved in hydrogen bonding with water.

The most-populated conformation was subjected to multiple blind docking experiments on Hsp90 using the Autodock program.[12] In all cases, the peptide was predicted to bind within the ATP binding site of Hsp90 (Figure 1A−C). Analysis of the blind docking results through the procedure described by Hetenyi et al.[27] showed that low-energy poses are all closely correlated with one another, with an rmsd from the global minimum structure lower than 2.5 Å. Control docking experiments were conducted with the extended structures representative of other clusters, but in those cases it was not possible to univocally identify any particular binding site on Hsp90.

The free-energy minimum structure of the Hsp90/shepherdin complex was then subjected to two long, 54 and 73 ns, all-atom MD simulations. Analysis of the statistical and time-dependent distribution of the interactions between functional groups of the ligand and of the chaperone was carried out to develop pharmacophore models, keeping into account the motional and flexibility properties of both the ligand and the receptor. Shepherdin partially reoriented to increase the total number of stabilizing contacts with the ATP binding pocket of Hsp90 (Figure 1A−D). Attention was focused in particular on the analysis of hydrogen-bonding, hydrophobic/aromatic, and charge−charge interactions, as these represent the most common types of intermolecular forces determining host/guest recognition in drugs.

The functional groups of shepherdin involved in direct or water-mediated hydrogen bonds with the binding pocket of Hsp90 included the γ-OH functions of Ser84, Ser85, and the imidazole ring of His86 (Figure 1B−D). The latter, in particular, could satisfy hydrogen-bonding conditions being involved in interactions both as an acceptor (Nϵ atom) and as a donor (Nδ-H

functional group; Figure 1C,D). The remaining hydrogen-bonding group on shepherdin, Cys82, was involved to a lesser extent in intermolecular H-bonding interactions; however, its presence was shown experimentally to be necessary to ensure binding. Moreover, it displayed hydrophobic interactions with the side chains of Hsp90, Leu108 and the alkyl part of Asn109. Cys82 is also important for preserving the hairpin structure; mutations to Ala on the isolated peptide lead to loss of ordered hairpin structure.[11]

To define the presence of hydrophobic/aromatic interactions, the contacts involving the side chains of Phe80 and His86 were monitored during simulation. Shepherdin Phe80 was found to be in contact mainly with the charged/polar side chains of Lys59, Asn52, and Asn55 on Hsp90, while shepherdin His86 was not significantly involved in hydrophobic/aromatic contacts with Hsp90 residues.

Finally, the role of the positively charged ammonium group on the side chain of shepherdin Lys87 was found to be only marginally involved in interactions with the backbone carbonyl oxygens of Hsp90 residues Phe135 and Gly136, being mostly exposed to the water solvent during MD simulations.

Pharmacophoric Hypotheses and Small Molecule Identification. Three different pharmacophore models were built and labeled PHARM1, PHARM2, and PHARM3 based on the results of MD simulations. The conformation of shepherdin and the orientations of its side-chain functional groups in the most populated structural cluster from MD trajectories of the complex were used as structural template (Figure 1C,E). The distributions of dihedral values (Table 1) and distances (Table 2) among critical functionalities were used to define upper and lower boundaries for geometric constraints.

PHARM1 (Figure 1E) consisted of four pharmacophoric points: three H-bonding donor functionalities mapped over the side chain OH group of Ser84, Ser85, and the SH group of the Cys82, plus one imidazole ring moiety mapped on the position of the corresponding ring of His86 (Figure 1E). Each imidazole atom was allowed to bear any substituent or be a bridgehead in the presence of a fused ring. PHARM2 consisted of two H-bonding donor groups corresponding to the γ-OH of Ser84 and Ser85, one aromatic function centered on the position of the Phe80 benzene ring, and one hydrophobic function centered on the S atom of Cys82. PHARM3 had the same properties as PHARM1, augmented by the presence of a positive charge mapped on the position of the ammonium group of Lys87.

The three models described above were used as queries for a search of the NCI_3D database of molecules (containing approximately 160 000 compounds). The search with PHARM1 yielded 73 compounds, the search with PHARM2 yielded 42 compounds, while PHARM3 gave no hits. In experimental tests, the molecules corresponding to hits of PHARM2 proved to be extremely insoluble due to the presence of aromatic/hydrophobic groups and thus had no tumor-cell-killing effect. The search with PHARM1 yielded, among others, 20 hits reminiscent of the class of known purine-based inhibitors of the ATP-binding pocket of Hsp90.[28,29] Interestingly, one of the nonpurine-based hits that was found to be effective in experiments, AICAR (Figure 1E),[25] was not previously known to interfere with Hsp90 chaperone functions and was characterized by a novel molecular structure among Hsp90 antagonists.

Molecular Interactions between AICAR and Hsp90: MD Simulation Results. The structure of the complex between AICAR and Hsp90, obtained with the docking procedure described in Materials and Methods, was studied in solution by MD simulations in explicit water solvent. The 100 ns time
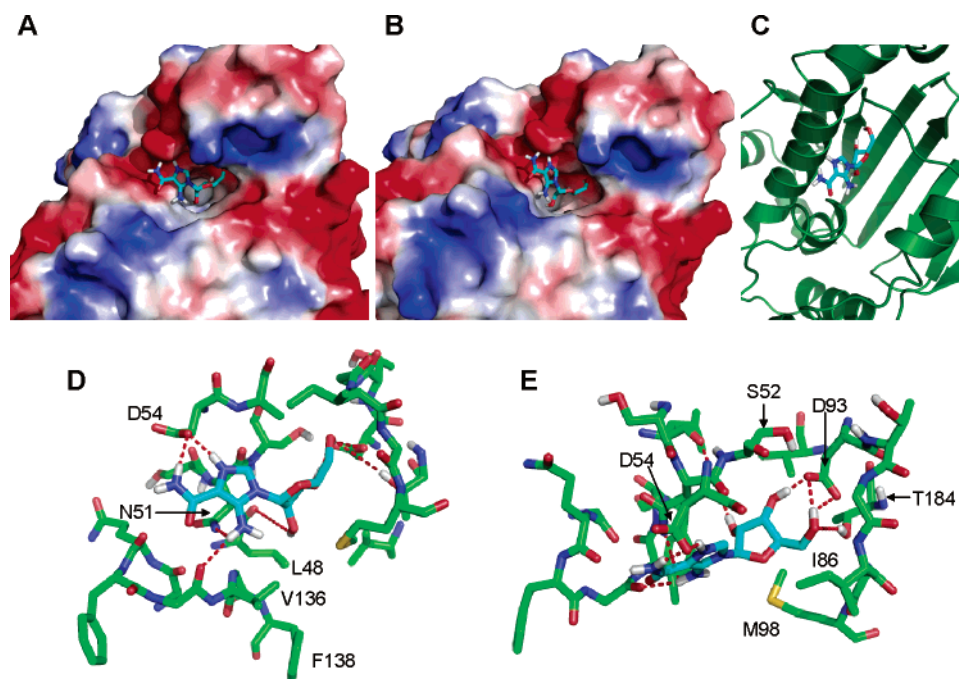
Figure 2. Molecular interactions in the AICAR/Hsp90 complex. (A) Structure of the MD-refined docked complex between AICAR and the N-domain of Hsp90. The ligand is represented by sticks, while the protein is represented by its Van der Waals surface, colored according to its electrostatic potential: red indicates regions of negative charge, white indicates hydrophobic regions, and blue indicates positively charged regions. (B) Same as (A) but with a different orientation. (C) Structure of the MD-refined docked complex between AICAR and the N-domain of Hsp90. The protein is represented by its secondary structure. (D, E) Two different orientations of the Hsp90 binding site with AICAR bound. The main interactions between AICAR and Hsp90 residues are highlighted. The carbon atoms of AICAR are colored light blue.
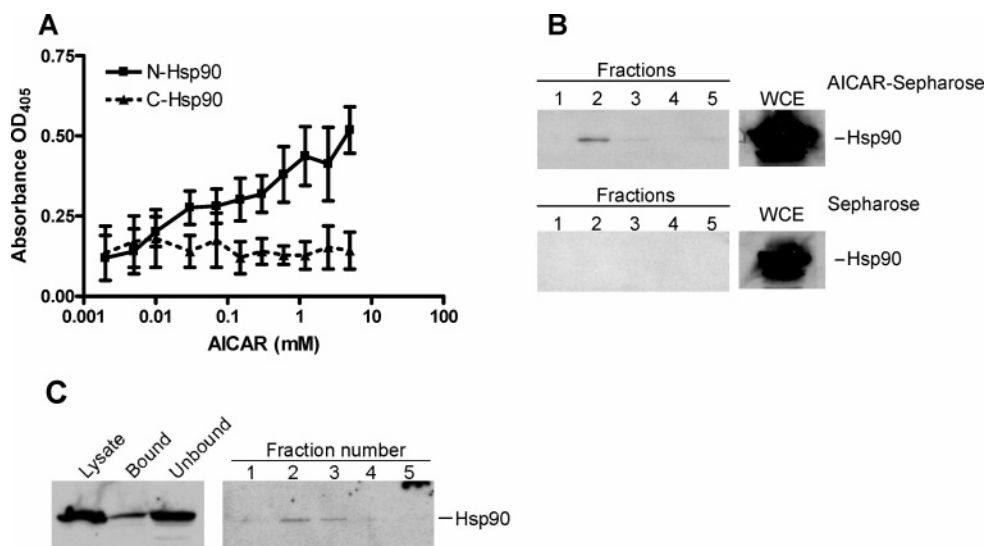

Figure 3. Binding of AICAR to Hsp90. (A) ELISA. Microtiter wells were coated with the indicated increasing concentrations of AICAR and incubated with recombinant N- or C-domain of Hsp90. Binding was determined using domain-specific antibodies to Hsp90 and quantified by absorbance at OD_{405}. Data are the mean ± SEM of three independent experiments. (B) Affinity chromatography. AICAR was coupled to sepharose and used to fractionate HeLa cell extracts. Eluted fractions were analyzed by Western blotting. A sepharose column was used as control. (C) Competition between shepherdin and AICAR. Cell extracts are fractionated on a sepharose−shepherdin column. The bound material was then eluted with soluble AICAR (5 mg/mL), and the resulting fractions were Western Blotted for Hsp90. Hsp90 was eluted from the column using AICAR.

length reported for this simulation represents, to the best of our knowledge, the first case where such time scales have been accessed and used for the study of systems of this degree of complexity. Analysis of the trajectory shows that AICAR docks into the ATP-binding pocket of Hsp90 (Figure 2A−C) and that it is involved in several direct hydrogen-bonding contacts with the residues of the Hsp90 ATP-binding pocket. The five-member sugar ring fits nicely into a pocket flanked by negatively charged and hydrophobic regions (Figure 2A,B). The OH group in position 2 on the ribose points into a deep hydrophobic channel defined by the side chains of Leu48, Met98, Val136, Phe138, and Val186. In this binding mode, AICAR is also involved in direct hydrogen-bonding contacts with the side chain of Asp93, through the OH groups in positions 3 and 5 of the ribose ring (Figure 2D,E). Interestingly, the interaction with Asp93 was already defined as specific for the shepherdin/Hsp90 complex and is also characteristic of the interaction of the chaperone with the anticancer molecule radicicol and some of its derivatives.[30] The hydroxyl group in position 3 is also involved as a hydrogen bond acceptor with the side chain of Ser52.
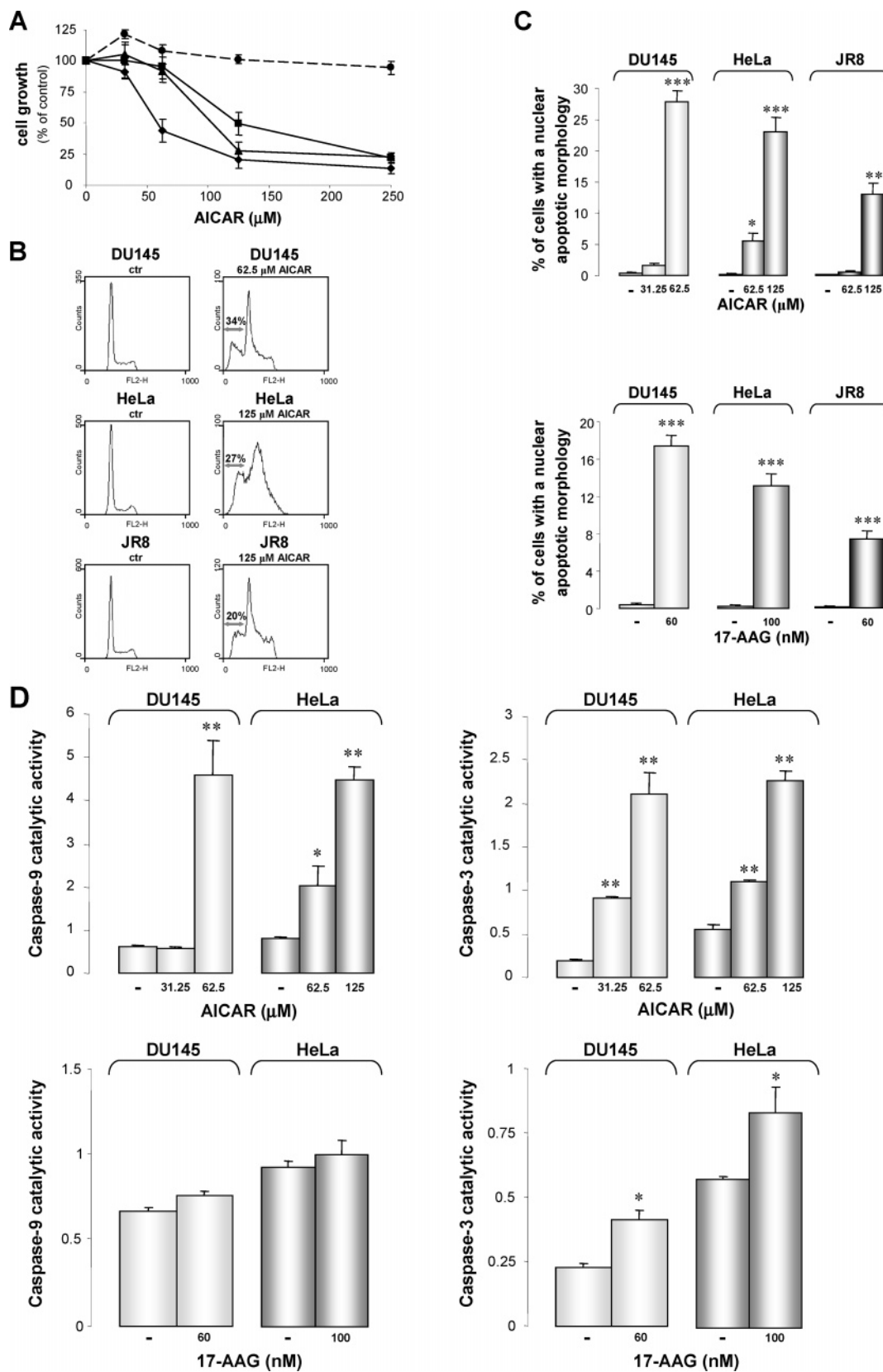
Figure 4. Inhibition of cell proliferation and induction of apoptosis by AICAR in tumor cell lines. (A) Inhibition of cell proliferation in DU145 (◆), Hela (■), JR8 (▲), and WI38 (●) cells, as evaluated by cell counting after a 72-h exposure to AICAR. Values represent the mean (±SD) of three independent experiments. (B) DNA content analysis. DU145, HeLa, and JR8 cells were treated with AICAR or 17-AAG for 72 h, harvested and analyzed for DNA content by flow cytometry. The percentage of the apoptotic sub-$G_{0/1}$ population is reported in each histogram. (C) Fluorescence microscopy analysis. The percentage of cells with an apoptotic morphology was assessed by fluorescence microscopy after exposure of cells to AICAR or 17-AAG for 72 h. Data represent the mean values (±SD) of three independent experiments, $P < 0.01$, $P < 0.02$, and $P < 0.05$, student's t test. (D) Caspase activation. Caspase-9 and caspase-3 catalytic activity was determined by hydrolysis of the fluorogenic substrate LEHD-pNA and DEVD-pNA, respectively, in cells exposed to AICAR for 72 h. Data represent the mean values (±SD) of three independent experiments, $P < 0.01$, $P < 0.05$, and student's t test.

Table 3. Cytotoxic Activity of AICAR and 17-AAG in Tumor Cell Lines[a]

cell line	AICAR IC_{50} (μM)	17-AAG IC_{50} (μM)
DU145	59.0 ± 8.5	68.3 ± 5.8
HeLa	126.0 ± 10.3	108.2 ± 19.3
JR8	105.0 ± 7.7	53.3 ± 4.9

[a] Drug activity is expressed in terms of the concentration able to inhibit cell growth by 50% (IC_{50}). Values represent the mean ± SD of three independent experiments.

The imidazole moiety points toward a negatively charged region of the Hsp90 ATP-binding side, characterized by the presence of Asp54 and Asn51. The acidic hydrogens on the aromatic nitrogen atom in position 3 and on the carboxamide at position 4 of the imidazole are directly involved in stabilizing interactions with the carboxylate group of Asp54, while the NH_2 group on imidazole position 5 acts as a hydrogen-bonding acceptor with respect to the side chain amide group of Asn51 and donates one hydrogen bond to the carbonyl group of Gly125.

Finally, it is worth noting that the regions of the protein that display the highest fluctuations and undergo secondary structure rearrangements include residues 65−75 and 105−112 and are directly in contact with the active site region of the protein (see Supporting Information Figure S3). The latter adapts dynamically to the presence of the ligand, which in turn finds the optimal sterical and chemical fitting within the ATP binding pocket. These observations are consistent with the results of recent X-ray studies of Hsp90 in complex with different ligands reported by Wright et al.[31]

Molecular Interactions between AICAR and Hsp90: Experimental Tests. ELISA showed that AICAR bound the recombinant Hsp90 N-domain in a specific and saturable manner, whereas no specific binding of AICAR to the C-terminus region of Hsp90 was demonstrated (Figure 3A). To further investigate the physical interaction between AICAR and Hsp90 in vivo, affinity chromatography experiments were carried out. Fractionation of HeLa cell extracts over an AICAR-Sepharose column resulted in the isolation of Hsp90 by Western blotting of eluted fractions (Figure 3B,C). In contrast, no specific association of Hsp90 with a control Sepharose column was observed (Figure 3B,C).

AICAR Induces Tumor Cell Death. A 72-h exposure to different concentrations (from 31.25 to 250 μM) of AICAR induced a dose-dependent decline in cell proliferation in various human tumor cell lines tested (Figure 4A). Specifically, the 50% inhibitory concentration (IC_{50}) values, as calculated from the growth curves, were 59.0 ± 8.5 μM, 105.0 ± 7.7 μM, and 126.0 ± 10.3 μM for the DU145, JR8, and HeLa cell lines, respectively (Table 3). In contrast, identical concentrations of AICAR did not reduce the growth of WI38 normal human lung fibroblasts (Figure 4A). For comparative purposes, the antiproliferative effect of 17-AAG was also evaluated and IC_{50} values ranging from 53.3 ± 4.1 nM to 108.2 ± 19.3 nM were observed for the different cell lines (Table 3). In tumor cell lines, AICAR induced the activation of apoptosis, as demonstrated by the appearance of an apoptotic sub-$G_{0/1}$ peak after a 72-h exposure to the drug (Figure 4B). Such a peak, which was not appreciable in untreated cells, accounted for 34.0 ± 2.3% of the overall cell population in DU145 cells treated with 62.5 μM AICAR and for 27.0 ± 1.4% and 20.0 ± 6.1%, respectively, in HeLa and JR8 cells treated with the highest (125 μM) drug concentration. Genuine induction of tumor cell apoptosis by AICAR was also confirmed by a significant increase in the percentage of

cells with an apoptotic nuclear morphology, as detected by fluorescence microscopy after cell staining with propidium iodide (Figure 4C). In these experiments, spontaneous apoptosis was negligible (0.15−0.44% in different cell lines), whereas AICAR treatment increased the apoptotic rate in a concentration-dependent manner. Maximum peaks of 28 ± 1.7, 23 ± 2.4, and 13 ± 1.8% were observed in DU145, HeLa, and JR8, respectively, following exposure to AICAR concentrations around the IC_{50} values of each cell line. Exposure to equitoxic (∼IC_{50}) 17-AAG concentrations resulted in an apoptotic rate of 15.9 ± 2.0, 10.8 ± 1.5, and 12.0 ± 1.9% in DU145, HeLa, and JR8, respectively (Figure 4C). AICAR-induced tumor cell apoptosis was accompanied by a significant increase in capase-9 and capase-3 catalytic activity, as assessed by the in vitro hydrolysis of specific fluorogenic substrates (Figure 4D). Although to a lesser extent, significant activation of caspase-3 was also observed in DU145 and HeLa cells following 17-AAG exposure. Conversely, a negligible drug effect on caspase-9 activity was recorded (Figure 4D).

AICAR Inhibits Hsp90 Chaperone Function. We next asked whether the cytotoxic effect exerted by AICAR was due to the breakdown of multiple cell survival pathways as a consequence of destabilization of Hsp90 client proteins. AICAR-treated DU145 and HeLa cells exhibited reduced expression of the Hsp90 client proteins Neu, Akt, and CDK-6 and almost complete loss of survivin by Western blotting (Figure 5A). In contrast, AICAR did not affect Hsp90 and Hsp70 expression (Figure 5A). Exposure of DU145 cells to 17-AAG resulted in almost complete abrogation of the Hsp90 client protein Raf-1 and a marked decline in Neu. Conversely, no appreciable inhibition of survivin expression was detected. 17-AAG did not modify the Hsp90 expression level, but markedly increased Hsp70 protein abundance (Figure 5A). In addition, immune complexes precipitated from extracts of AICAR-treated tumor cells revealed a 70% reduction in telomerase activity, which requires Hsp90 chaperone function,[32] as compared with control incubation reactions (Figure 5B,C).

Discussion

In this study, we used a structure- and dynamics-based rational design to identify the nonpeptidic small molecule AICAR as a structurally novel inhibitor of Hsp90 (Figure 1E). The compound was selected to engage the ATP-binding pocket of the N-terminal domain of Hsp90, with binding and functional properties that mimic those of the peptidic antagonist of the survivin-Hsp90 complex, shepherdin.[11] Accordingly, AICAR bound the Hsp90 N-domain, destabilized multiple Hsp90 client proteins in vivo, including survivin, and exhibited broad antiproliferative activity in multiple tumor cell lines, although at higher concentrations than those required to obtain the same growth inhibitory effect with 17-AAG, with induction of apoptosis and inhibition of cell proliferation. Reminiscent of the selective anticancer activity of shepherdin, AICAR did not affect proliferation of normal human fibroblasts.

Hsp90 is generally viewed as a "druggable" target for rational cancer therapy because of its role at the crossroads of multiple signaling pathways associated with cell proliferation and cell viability and its elevated ATPase activity in tumors as opposed to normal tissues, which may provide a favorable therapeutic window.[5,33] This has prompted considerable interest in the development of Hsp90 antagonists for clinical use, a strategy that relied largely on the macrocyclic antibiotic Geldanamycin (GA) and its 17-allyl derivative, 17-AAG, as template structures.[13,33−35] Conversely, the pharmacophore strategy pre-
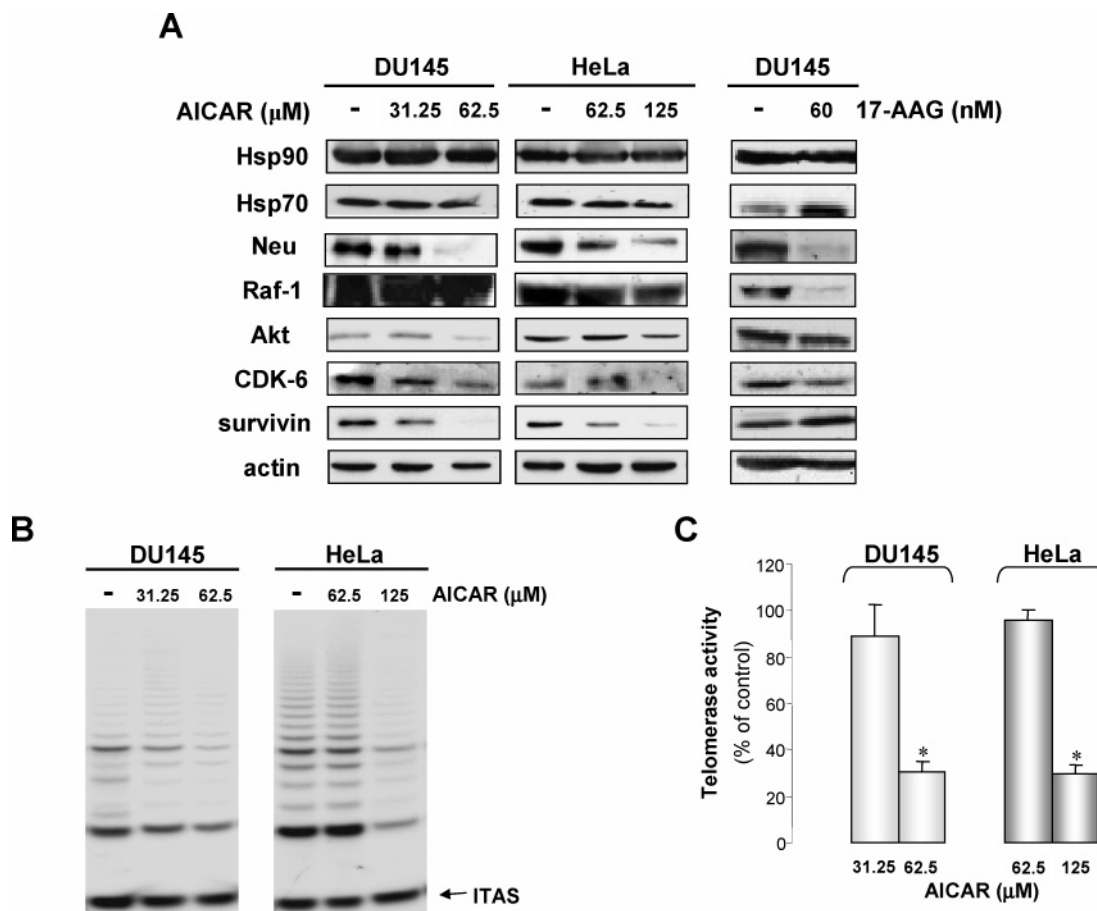
Figure 5. AICAR inhibits Hsp90 chaperone function. (A) Loss of Hsp90 client proteins in cancer cells treated with AICAR or 17-AAG for 72 h and analyzed by Western blotting. (B−C) Telomerase activity. Hsp90 was immunoprecipitated from AICAR-treated DU145 and HeLa cells, and telomerase activity was determined by TRAP assay. ITAS, internal amplification standard. Data represent the mean values ($\pm$SD) of three independent experiments. $P < 0.01$, student's t test.

sented here, using the shepherdin peptidomimetic as a lead structure, uncovered an unexpected degree of molecular and structural heterogeneity for Hsp90 inhibitors and identified AICAR as a novel antagonist of the chaperone ATPase activity with promising anticancer activity. It is worth noting that the molecular structure of AICAR is totally uncorrelated with that of ansamycins. The former features a ribose ring linked to a heterocyclic imidazole function mimicking the aromatic portion of His86 and provides easy access to several functional groups for further chemical modification, while the latter is generally characterized by an aliphatic macrocycle linking nonadjacent positions of an aromatic ring. Similarly to shepherdin,[11] preliminary docking studies predicted AICAR to engage the ATPase pocket of Hsp90 differently from GA, and amino acids that contact GA were predicted by simulation analysis to be marginally involved or not involved at all in shepherdin or AICAR docking to Hsp90.

Strengthening the rationale of the proposed shepherdin-based screening strategy, which takes into account the motional and flexibility properties of the complex with Hsp90 via all-atom MD, previous site-directed mutagenesis experiments confirmed the essential roles of the two Ser, His, and Cys residues in shepherdin that make up the pharmacophore used here. Moreover, a minimal shepherdin KHSSG sequence was sufficient to retain the ability to bind Hsp90 and exhibit selective anticancer activity.[36] Models generated based only on the initial semirigid docking results may not properly recapitulate flexible regions in Hsp90 required for inhibitor binding and failed to identify the groups essential for recognition.

In this context, the results of the AICAR/Hsp90 interaction studies presented here are indicative of the structural determinants for the activity of AICAR as an Hsp90 inhibitor. In particular, AICAR is involved in a direct contact with Asp93 through two hydroxyl groups on the furanoside, suggesting that modifications of these residues with other polar groups may actually strengthen the molecular recognition interaction. The same considerations hold for the substituents on the imidazole ring. Analysis of the structure of the complex after long time scale MD refinement also suggests other modifications aimed at improving the hydrophobic contribution to the free-energy of association: the hydroxyl group in position 2 of the furanoside points directly toward a hydrophobic channel that can be occupied by a hydrophobic moiety.

In previous studies, AICAR has been proposed as a pharmacological activator of AMP-activated protein kinase (AMPK), with potential anti-inflammatory properties.[37,38] The recently described anticancer activity of AICAR was attributed to this molecular recognition and, in particular, to inhibition of PI3 kinase-Akt signaling, with increased expression of cyclin-dependent kinase inhibitors, p21, p27, and p53.[39] Our data suggest an additional function of AICAR as a novel and structurally diverse Hsp90 antagonist, and its anticancer activity reflects inhibition of the chaperone function with destabilization of multiple Hsp90 client proteins, including Neu, CDK6, Akt, survivin, and telomerase. It is worthy of note that the molecular mechanisms by which AICAR exerts its activity are not superimposable to those of 17-AAG. In fact, we failed to evidence an inhibitory effect on survivin expression after cell

exposure to a cytotoxic concentration (IC$_{50}$) of 17-AAG. This finding is in accord with previous data from our group showing a decline of survivin protein expression in prostate cancer cells only starting from a very high 17-AAG concentration (>850 nM).[40] Moreover, at variance with 17-AAG, AICAR did not modify the expression of Hsp70 and Raf-1 proteins.

It has to be stressed that our data do not exclude the interference of AICAR with the AMPK pathway, but suggest its possible parallel interaction in the cell with a different biological pathway exploited in cancer. Most importantly, the cell killing effect of AICAR is selective, as the drug spares normal cells.

The strategy proposed here can be extended to the investigation of other targets involved in cancer development and to the identification of possible new uses for already known drugs.

In summary, we have presented a novel, simple, and general design strategy based on the combination of docking and all-atom MD refinement to identify the binding determinants of complex formation while keeping flexibility into account. This protocol was applied to study the interaction between a novel peptidomimetic antagonist of the survivin−Hsp90 complex, shepherdin, and Hsp90. Our approach allowed us to explore the molecular diversity space of Hsp90 inhibitors and to rationally identify a new structural antagonist, AICAR. The ability to inhibit the chaperone function, destabilize multiple client proteins in vivo, and exhibit selective anticancer activity makes AICAR a viable lead structure for the further development and refinement of novel Hsp90 antagonists structurally different from 17-AAG.

Supporting Information Available: Figure S1 reports the structure of the Hsp90/shepherdin complex after 70 ns of all-atom MD (Figure S1A) and the evolution in time of the number of intermolecular hydrogen-bonding interactions (Figure S1B). Figure S2 reports the structure of the first five docked conformations of shepherdin from the absolute free-energy minimum (Figure S2A) and the results of clustering on the whole set of docked conformations (Figure S2B). Figure S3 reports the time evolution of the secondary structure of Hsp90 in complex with AICAR. This material is available free of charge via the Internet at http://pubs.acs.org.

References

(1) Vogelstein, B.; Kinzler, K. W. Cancer genes and the pathways they control. *Nat. Med.* **2004**, *10*, 789−799.

(2) O'Dwyer, M. E.; Druker, B. J. Status of Bcr-Abl tyrosine kinase inhibitors in chronic myelogenous leukemia. *Curr. Opin. Oncol.* **2000**, *12* (6), 594−597.

(3) O'Dwyer, M. E.; Druker, B. J. STI571: An inhibitor of the BCR-ABL tyrosine kinase for the treatment of chronic myelogenous leukemia. *Lancet Oncol.* **2000**, *1*, 207−211.

(4) Paez, J. G.; Janne, P. A.; Lee, J. C.; Tracy, S.; Greulich, H.; Gabriel, S.; Herman, P.; Kaye, F. J.; Lindeman, N.; Boggon, T. J.; Naoki, K.; Sasaki, H.; Fujii, Y.; Eck, M. J.; Sellers, W. R.; Johnson, B. E.; Meyerson, M. EGFR mutations in lung cancer: Correlation with clinical response to gefitinib therapy *Science* **2004**, *304*, 1497−1500.

(5) Whitesell, L.; Lindquist, S. L. Hsp90 and the chaperoning of cancer. *Nat. Rev. Cancer* **2005**, *5*, 761−772.

(6) Young, J. C.; Moarefi, I.; Hartl, F. U. Hsp90: A specialized but essential protein-folding tool. *J. Cell Biol.* **2001**, *154*, 267−273.

(7) Neckers, L.; Ivy, S. P. Heat shock protein 90. *Curr. Opin. Oncol.* **2003**, *15*, 419−424.

(8) Workman, P. Overview: Translating Hsp90 biology into Hsp90 drugs. *Curr. Cancer Drug Targets* **2003**, *3* (5), 297−300.

(9) Altieri, D. C. Validating survivin as a cancer therapeutic target. *Nat. Rev. Cancer* **2003**, *3*, 46−54.

(10) Fortugno, P.; Beltrami, E.; Plescia, J.; Fontana, J.; Pradhan, D.; Marchisio, P. C.; Sessa, W. C.; Altieri, D. C. Regulation of survivin function by Hsp90. *Proc. Natl. Acad. Sci. U.S.A.* **2003**, *100*, 13791−13796.

(11) Plescia, J.; Salz, W.; Xia, F.; Pennati, M.; Zaffaroni, N.; Daidone, M. G.; Meli, M.; Dohi, T.; Fortugno, P.; Nefedova, Y.; Gabrilovich, D. I.; Colombo, G.; Altieri, D. C. Rational design of Shepherdin, a novel anticancer agent. *Cancer Cell* **2005**, *7*, 457−467.

(12) Morris, G. M.; Goodsell, D. S.; Halliday, R. S.; Huey, R.; Hart, W. E.; Belew, R. K.; Olson, A. J. Automated docking using a lamarckian genetic algorithm and empirical binding free energy function. *J. Comput. Chem.* **1998**, *19*, 1639−1662.

(13) Stebbins, C. E.; Russo, A. A.; Schneider, C.; Rosen, N.; Hartl, F. U.; Pavletich, N. P. Crystal structure of Hsp90−geldanamycin complex: Targeting of a protein chaperone by an antitumor agent. *Cell* **1997**, *89*, 239−250.

(14) Mehler, E. L.; Solmajer, T. Electrostatic effects in proteins. Comparison of dielectric and charge models. *Protein Eng.* **1991**, *4* (8), 903−910.

(15) Berendsen, H. J. C.; Postma, J. P. M.; van Gunsteren, W. F.; Di Nola, A.; Haak, J. R. Molecular dynamics with coupling to an external bath. *J. Chem. Phys.* **1984**, *81*, 3684.

(16) van Gunsteren, W. F.; Daura, X.; Mark, A. E. GROMOS Force Field. *Encycl. Comput. Chem.* **1998**, *2*, 1211−1216.

(17) van Gunsteren, W. F.; Billeter, S. R.; Eising, A. A.; Hunenberger, P. H.; Kruger, P.; Mark, A. E.; Scott, W. R. P.; Tironi, I. G. *The GROMOS96 Manual and User Guide*. In vdf Hochschulverlag, ETH Zurich: Switzerland, 1996.

(18) Berendsen, H. J. C.; Grigera, J. R.; Straatsma, T. P. The missing term in effective pair potentials. *J. Phys. Chem.* **1987**, *91*, 6269−6271.

(19) Hess, B.; Bekker, H.; Fraaije, J. G. E. M.; Berendsen, H. J. C. A linear constraint solver for molecular simulations. *J. Comput. Chem.* **1997**, *18*, 1463−1472.

(20) Miyamoto, S.; Kollman, P. A. SETTLE: An analytical version of the SHAKE and RATTLE algorithms for rigid water models. *J. Comput. Chem.* **1992**, *13*, 952−962.

(21) Darden, T.; York, D.; Pedersen, L. Particle mesh Ewald: An N-log(N) method for Ewald sums in large systems. *J. Chem. Phys.* **1993**, *98*, 10089−10092.

(22) van der Spoel, D.; Lindahl, E.; Hess, B.; van Buuren, A. R.; Apol, E.; Meulenhoff, P. J.; Tieleman, D. P.; Sijbers, A. L. T. M.; Feenstra, K. A.; Drunen, R. v.; Berendsen, H. J. C. *Gromacs User Manual*, version 3.2; www.gromacs.org, 2004.

(23) Daura, X.; Jaun, B.; Seebach, D.; van Gunsteren, W. F.; Mark, A. E. Reversible peptide folding in solution by molecular dynamics simulation. *J. Mol. Biol.* **1998**, *280*, 925−932.

(24) *Catalyst*; Accelrys: San Diego, CA, 2005.

(25) Ferris, J. P.; Devadas, B.; Huang, C. H.; Ren, W. Y. Nucleosides from carbohydrate adducts of diaminomaleonitrile. A novel synthesis of 5-amino-1-(beta-D-ribofuranosyl)imidazole-4-carboxamide and 5-amino-1-(beta-D-ribopyranosyl)imidazole-4-carboxamide. *J. Org. Chem.* **1985**, *50* (6), 747−754.

(26) Folini, M.; Brambilla, C.; Villa, R.; Gandellini, P.; Vignati, S.; Paduano, F.; Daidone, M. G.; Zaffaroni, N. Antisense oligonucleotide-mediated inhibition of hTERT, but not hTERC, induces rapid cell growth decline and apoptosis in the absence of telomere shortening in human prostate cancer cells *Eur. J. Cancer* **2005**, *41* (4), 624−634.

(27) Hetenyi, C.; van der Spoel, D. Efficient docking of peptides to proteins without prior knowledge of the binding site. *Protein Sci.* **2002**, *11*, 1729−1737.

(28) Vilenchik, M.; Solit, D.; Basso, A.; Huezo, H.; Lucas, B.; He, H.; Rosen, N.; Spampinato, C.; Modrich, P.; Chiosis, G. Targeting wide-range oncogenic transformation via PU24FCL, a specific inhibitor of tumor Hsp90. *Chem. Biol.* **2004**, *11*, 787−797.

(29) Chiosis, G.; Lucas, B.; Shtil, A.; Huezo, H.; Rosen, N. Development of a purine-scaffold novel class of Hsp90 binders that inhibit the proliferation of cancer cells and induce the degradation of Her2 tyrosine kinase. *Bioorg. Med. Chem.* **2002**, *10*, 3555−3564.

(30) Dymock, B. W.; Barril, X.; Brough, P. A.; Cansfield, J. E.; Massey, A.; McDonald, E.; Hubbard, R. E.; Surgenor, A.; Roughley, S. D.; Webb, P.; Workman, P.; Wright, L.; Drysdale, M. J. Novel, potent small-molecule inhibitors of the molecular chaperone Hsp90 discovered through structure-based design. *J. Med. Chem.* **2005**, *48* (13), 4212−4215.

(31) Wright, L.; Barril, X.; Dymock, B.; Sheridan, L.; Surgenor, A.; Beswick, M.; Drysdale, M.; Collier, A.; Massey, A.; Davies, N.; Fink, A.; Fromont, C.; Aherne, W.; Boxall, K.; Sharp, S.; Workman, P.; Hubbard, R. E. Structure−activity relationships in purine-based inhibitor binding to Hsp90 isoforms. *Chem. Biol.* **2004**, *11*, 775−785.

(32) Holt, S. E.; Aisner, D. L.; Baur, J.; Tesmer, V. M.; Dy, M.; Ouellette, M.; Trager, J. B.; Morin, G. B.; Toft, D. O.; Shay, J. W.; Wright, W. E.; White, M. A. Functional requirement of p23 and Hsp90 in telomerase complexes *Genes Dev.* **1999**, *13* (7), 817−826.

(33) Janin, Y. L. Heat shock protein 90 inhibitors. A text book example of medicinal chemistry? *J. Med. Chem.* **2005**, *48* (24), 7503−7512.

(34) Roe, S. M.; Prodromou, C.; O'Brien, R.; Ladbury, J. E.; Piper, P. W.; Pearl, L. H. Structural basis for inhibition of the Hsp90 molecular chaperone by the antitumor antibiotics radicicol and geldanamycin. *J. Med. Chem.* **1999**, *42*, 260−266.

(35) Sausville, E. A. Geldanamycin analogs. *J. Chemother.* **2004**, *16* (S4), 68−69.

(36) Gyurkocza, B.; Plescia, J.; Raskett, G. M.; Garlick, D. S.; Lowry, P. A.; Carter, B. Z.; Andreeff, M.; Meli, M.; Colombo, G.; Altieri, D. C. Antileukemic activity of shepherdin and molecular diversity of Hsp90 inhibitors. *J. Natl. Cancer Inst.* **2006**, *98* (15), 1068−1077.

(37) Giri, S.; Nath, N.; Smith, B.; Viollet, B.; Singh, A. K.; Singh, I. 5-Aminoimidazole-4-carboxamide-1-beta-4-ribofuranoside inhibits proinflammatory response in glial cells: A possible role of AMP-activated protein kinase. *J. Neurosci.* **2004**, *24* (2), 479−487.

(38) Nath, N.; Giri, S.; Prasad, R.; Salem, M. L.; Singh, A. K.; Singh, I. 5-Aminoimidazole-4-carboxamide ribonucleoside: A novel immuno-modulator with therapeutic efficacy in experimental autoimmune encephalomyelitis *J. Immunol.* **2005**, *175* (1), 566−574.

(39) Rattan, R.; Giri, S.; Singh, A. K.; Singh, I. 5-Aminoimidazole-4-carboxamide-1-beta-D-ribofuranoside inhibits cancer cell proliferation in vitro and in vivo via AMP-activated protein kinase. *J. Biol. Chem.* **2005**, *280* (47), 39582−39593.

(40) Paduano, F.; Villa, R.; Pennati, M.; Folini, M.; Binda, M.; Daidone, M. G.; Zaffaroni, N. Silencing of survivin gene by small interfering RNAs produces supra-additive growth suppression in combination with 17-allylamino-17-demethoxygeldanamycin in human prostate cancer cells. *Mol. Cancer Ther.* **2006**, *5* (1), 179−186.